Kõrgesaar, Mihkel; Kujala, Pentti; Romanoff, Jani

Load carrying capacity of ice-strengthened frames under idealized ice load and boundary conditions

Published in:
Marine Structures

DOI:
10.1016/j.marstruc.2017.10.011

Published: 01/03/2018

Document Version
Publisher's PDF, also known as Version of record

Marine Structures 58 (2018) 18–30

Contents lists available at ScienceDirect

Marine Structures

journal homepage: www.elsevier.com/locate/marstruc

Load carrying capacity of ice-strengthened frames under idealized ice load and boundary conditions

Mihkel Kõrgesaar*, Pentti Kujala, Jani Romanoff

Aalto University, Department of Mechanical Engineering, Otakaari 3, 00076 Aalto, Finland

ARTICLE INFO

Keywords:
Ship structures
Ice loads
Numerical simulations
Fracture
Limit states

ABSTRACT

Overload response of the stiffening frames in ship side structure due to ice loading is an important design consideration for ships operating in ice infested waters. By overload, we mean loads that are larger than assumed by the rules. Therefore, the response of ice strengthened grillage frames is investigated under a range of idealized rectangular pressure patches and by assuming different boundary conditions for the structural units. A flat, representative grillage of an ice-strengthened ship is considered and analysed using non-linear Finite Element Method. The response of the grillage frames is compared with the isolated frame response. Two frame types are considered: flatbars and L-frames. Finite element simulations revealed that patch length has strong effect on the frame deformation mode. The key characteristic that differentiates the response under shorter and longer patches is the longitudinal membrane stretching of the shell plating. Longer patches tend to suppress this deformation mode that leads to similar frame behaviour observed in isolated frame analysis. It is further shown that overload capacity of grillage frames reduces with increasing patch length to levels observed in isolated frame analysis. Analysis of plastic strain development in the frames and plating revealed that plastic strain localized faster in frames, but shell plating is more sensitive to patch height variations. This renders frames more susceptible to fracture than plating. Finally, the local failure mechanisms of the L-frames tend to diminish the load sharing capability and so negatively affects the overload behaviour.

1. Introduction

In Finland, about 90% of export and 80% of import are transported by sea using ships [1]. Since the sea is freezing annually in the region (Bay of Bothnia and Gulf of Finland) the ice loads must be accounted for in the design of ship structures. Therefore, ships operating in the region during the season must comply with the Finnish-Swedish Ice Class Rules (FSICR [2]), which are considered as "industry standard" for designing ships for first-year ice environments, see Ref. [3]. According to Riska and Kämäräinen [3], the design point in current rules is reaching yield at least once per winter on shell plating or supporting secondary frames. In contrast, ships operating in multi-year ice conditions must comply with IACS polar rules [4], which allow observable plastic deformations to develop in the structure due to ice load, but do not specify any measurable permanent deformations. The principle difference between elastic and plastic design methodology is that for the same loading scenario and steel material behaviour, plastic design methodology leads to reduced scantlings compared with elastic design due to the formation of plastic mechanism.

Reduction of scantlings is important considering the increasing demand for energy and operational efficiency. Therefore, overdimensioning of ice-going ships should be avoided, because these ships compete with open-water ships during the open-water season

* Corresponding author.
E-mail address: mihkel.korgesaar@aalto.fi (M. Kõrgesaar).

https://doi.org/10.1016/j.marstruc.2017.10.011
Received 9 June 2017; Received in revised form 6 September 2017; Accepted 28 October 2017

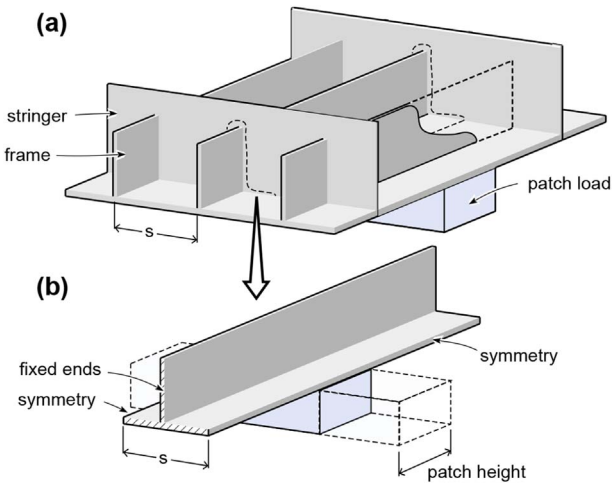

Fig. 1. (a) Frame as part of the grillage and the (b) isolated frame modelling approach.

[5]. This leads to a relevant question from design and economic perspective, which in the context of Arctic shipping can be formulated as in Ref. [6]: "*How low the ice class – and how close the ship can be to open water ship – to make the voyage without undue risks*". The question provides the incentive to explore the plastic design criteria as indicated in Fig. 1 since plastic behaviour of structures has been recognized to be essential in a rational ship design method in recent years, e.g. see the discussion in Refs. [7,8]. However, plastic deformations, as opposed to elastic deformations, are associated with a permanent set and non-linear structural response. The intertwining effects between load, the degradation of material due to corrosion, non-linear material behaviour, and consequent frame response in the grillage, up to the point of structural limit states are relatively unexplored territory in the context of ice strengthened ship structures. As discussed by Wang et al. [8,9] these challenging aspects are also the main cause for unclear safety margin in ice strengthening design standards.

To fill this gap, the paper provides insight into the ice-induced overload response and plastic capacity of frames in transversally stiffened grillage. By overload, we mean loads that are larger than assumed by the rules. The behaviour of ice strengthened structures under overload situations has been studied using Finite Element Method as early as 1980, see Ref. [10]. More recently, Daley et al. [11] provided the relevant insight into the overload response of isolated flat-bar frames under ice loads (Fig. 2(b)). By consideration of a wide range of frames with different web height to thickness ratio they determined the critical slenderness threshold, which exceedance leads to unstable web buckling as opposed to more favourable stable, buckling-free bending of the frame. However, compared with the isolated frame where deformations are constrained with idealistic boundary conditions, the frame in grillage (Fig. 2(a)) can behave quite differently depending on the load re-distribution in the grillage due to plate bending and the actual boundary conditions at the location of web-frames. Furthermore, these works consider plastification and collapse of a frame, but do not attempt to analyse the fracture limit state due to ice induced pressure loads. Therefore, the objective of the current work is to shed light on the limit states with respect to buckling and fracture of ice strengthened ship structures when frames are modelled as part of the grillage compared with isolated modelling approach.

Considered grillage is a representative of IA Super class ship and consists of hull plating, web frames, stringers and stiffening frames. To simplify the analysis on failure modes, initial curvature of the plating is neglected. The IA Super ice class provides a

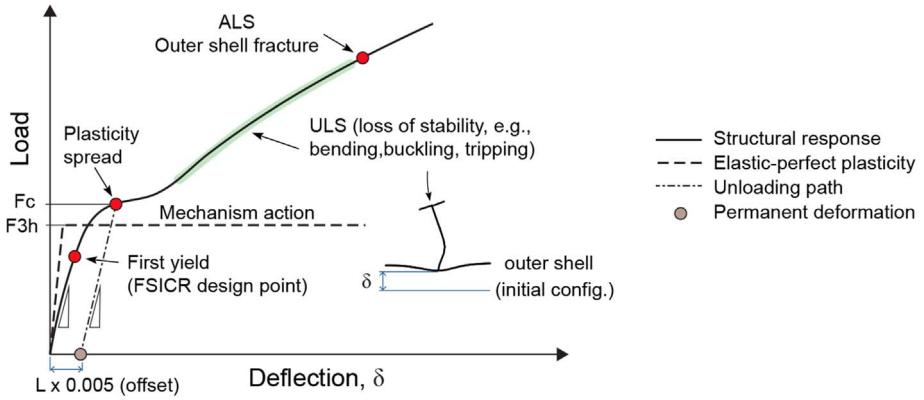

Fig. 2. Example of load-deflection curves for frames together with definitions used in this paper. Permanent deformation refers to inelastic, plastic deformation that is not recoverable and is measured on the outer shell at the location of frame.

strength equivalence between PC6 and PC7 class as shown in Ref. [12], thus results could be qualitatively extrapolated to these strength classes. Two alternative stiffening frames are considered: flatbars and L-profiles to demonstrate the influence of stiffener geometry on the non-linear failure process. A three-bay grillage model is loaded with the uniform rectangular pressure patch, which represents the rule-based ice load with the nominal contact area in compliance with the current design practice. Although the structural response has been shown in Refs. [13–16] to be sensitive to the pressure application method and patch size, the effect of the load patch on the response is considered in a simplified manner by treating only length and height of the pressure patch as variables. This supports identification of the main failure mechanisms, as in Ref. [17], uncoupled from actual complex ice-structure interaction process, which has been addressed elsewhere [18].

2. Limit states

According to ISO standard published in 2010 for design of Arctic offshore structures [19] the limit states relate to 100-year (10^{-2}) for ultimate (ULS) and 1000–100000 year (10^{-3} – 10^{-5}) extreme ice event for accidental limit state (ALS). Furthermore, the ALS design conditions for ice-structure interactions must include abnormal-level ice events (ALIE) with probability of 10^{-4}. In contrast, serviceability considerations are less important herein assuming that "hungry horse" look of the shell plating is acceptable and fixed on annual basis. Ultimate limit state can be defined in various ways. If material is assumed to follow elastic-perfect plasticity, ULS is achieved when the structure is converted into mechanism by the provision of suitable number and disposition of fully plastic zones [20]. Mechanism action implies that deformations increase infinitely without the load increase, see Fig. 2. Partly, this definition for ULS is adopted in design as it permits calculating the three-hinge collapse point for isolated frames using limit theory of plasticity and closed-form expressions. For instance, Daley [21] defined the three-hinge collapse pressure for centrally loaded beams

$$P_{3h} = \frac{(2 - k_w) + k_w\sqrt{1 - 48Z_{pns}(1 - k_w)}}{12Z_{pns}k_w^2 + 1}\frac{Z_p\sigma_y 4}{sbL(1 - h/(2L))} \tag{1}$$

where σ_y is the yield stress, k_w is the ratio of the web modulus to the full plastic modulus, Z_p is the plastic section modulus of frame assuming that plastic neutral axis is at the web-plate connection, s is the length of the applied pressure that is assumed equivalent with the frame spacing, h is the height of the load patch, L is the length of the frame, and Z_{pns} is a non-dimensional term given as

$$Z_{pns} = \left(\frac{Z_p}{A_w(L - h/2)}\right)^2 \tag{2}$$

where A_w is the area of the web. Note that in evaluating the 3-hinge pressure load, check was made that frames fail by 3-hinge mechanism, and not by shear at both supports.

In contrast to this idealistic condition, in reality the strain hardening of the material takes place. This has an effect of smooth spreading of plasticity instead of clearly developed yield lines with elastic zones between. Furthermore, significant portion of the load in a structure is carried by the membrane forces in stiffeners and plates that are not always accounted in the closed-form mechanism solution. Membrane and shear force further interact with bending and twisting moments in a plate, making redistribution of the loading two dimensional. Consequently, structure has an implicitly implied reserve capacity against this idealistic solution. To compare the three-hinge collapse load with the capacity load F_c of the structure as denoted in Fig. 2, the latter is sometimes determined using an offset method, see Refs. [11,22]. The assumption is that upon removing the load F_c, structure has sustained a permanent deformation equal to 0.5% of the frame length (e.g., 15 mm for 3 m long frame). This comparison is also performed here to determine the reserve capacity of a structure with respect to F_{3h}. Independent whether the lower load is given by F_c or F_{3h}, Fig. 2 implies that at these load levels structure still has additional reserve capacity against different collapse modes that can develop. Therefore, more generic definition is that ULS corresponds to situation where structure, or its parts, lose static equilibrium, but structure has still some reserve against rupture. This, somewhat vague definition has been also used in Fig. 2. Accidental limit state (ALS) on the other hand is explicitly defined in Fig. 2 as the point where the outer shell fracture occurs. To further point out the differences between ULS and ALS, Fig. 3 shows photographs of two damages in which ULS state has been reached including fracture in framing members, but no outer shell fracture took place.

3. Case study

3.1. Grillage structure

The initial dimensioning of the grillage structure was based on the M/T Uikku; structural details are given in Ref. [25]. Two modifications were introduced that leads to larger frames, see Table 1. The web height (h_w) to thickness (t_w) ratio was increased to increase the susceptibility to elasto-plastic buckling of the web, see e.g. Ref. [11]. Based on the parameters in Table 1 the transversally stiffened grillage structure can be fully defined according to FSICR as well as the design pressure that is given in Table 1. Therefore, calculated dimensions of frames, plating and larger load carrying members are given in Table 2. The compliance of frames against IACS Polar Class buckling requirements was checked as well. To avoid local buckling in the web of Polar Class vessels, IACS specifies that the ratio h_w/t_w is not to exceed the critical value:

- For flatbar sections: $h_w/t_{wn} \leq 282/(\sigma_y)^{0.5}$

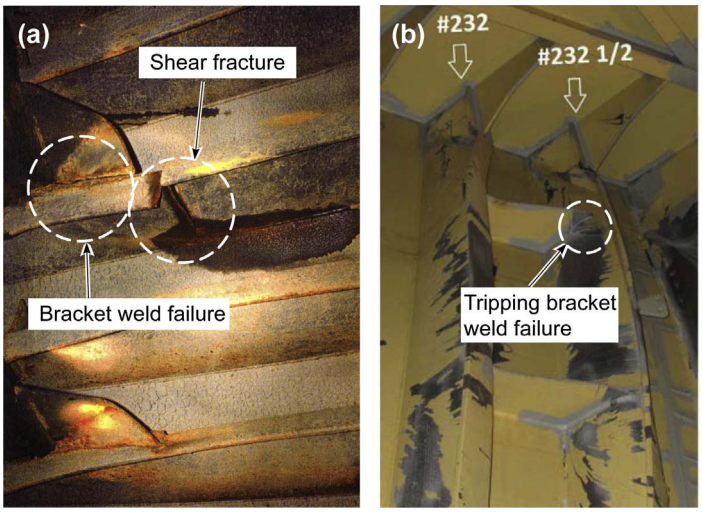

Fig. 3. Fracture in framing members as opposed to fracture in outer shell due to ice overload. (a) Bulk carrier – fracture due to shear at the upper end of the frame; figure from Ref. [23]. (b) Cargo carrier – tripping bracket weld failure as a result of frame tripping; Figure from Ref. [24].

Table 1
"Seed" dimensions according to M/T Uikku together with modified design parameters.

	M/T Uikku	Used design
Length, LPP	150 m	
Breadth, mould.	22.2 m	
Draught, design	9.5 m	
Deadweight	15748 t	
Displacement	22654 t	
Speed	17 kn	
Propulsion power	11.4 MW	
Frame spacing	0.35 m	0.4 m
Wep span	2.8 m	
Stringer span	2.5 m	3 m
Design pressure (FSICR)	3.44 MPa	

Table 2
Scantlings of grillage compliant with FSICR IA Super class.

	s	tp	hw	tw	bf	tf	Z req	Zcalc	Slenderness	Limit β	Limit β
	mm	mm	mm	mm	mm	mm	cm^3	cm^3	$h_w/t_w\,(\sigma_y/E)^{0.5}$	(IACS)	(Daley et al., 2017)
Flatbar	400	23.5	410	16	–	–	816	822	0.95	< 0.62	< 0.94
L	400	23.5	430	10.5	40	15	816	850	1.52	< 1.77	–

	Stringer				webframe			
	hw	tw	bf	tf	hw	tw	bf	tf
	mm	mm	mm	mm	mm	mm	mm	mm
Flatbar	660	18	140	20	800	22	140	24
L	660	18	140	20	800	22	140	24

*t_p – plate thickness, bf –flange breadth, t_f – flange thickness, Z_{req} – required (elastic) section modulus of frames, Z_{calc} – section modulus (elastic) of designed frames.

- For bulb, tee and angle sections: $h_w/t_{wn} \leq 805/(\sigma_y)^{0.5}$

Alternatively, the critical values can be expressed in terms of web slenderness ratio β

$$\beta = \frac{h_w}{t_w}\sqrt{\frac{\sigma_y}{E}} \tag{3}$$

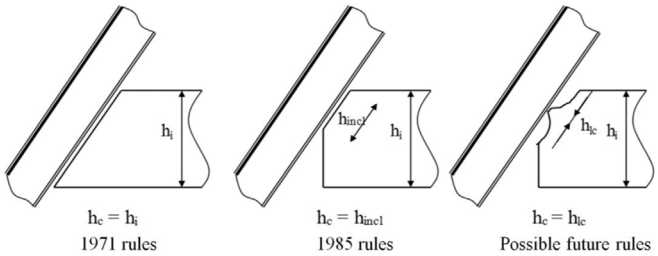

Fig. 4. Sketch of the concept of load height on a ship frame with different rule sets. Figure from Riska and Kämäräinen [3].

where $E = 206$ GPa is Young's modulus and $\sigma_y = 285$ MPa is the yield stress – values characteristic to normal shipbuilding steel used throughout this paper. By replacing the IACS h_w/t_w requirement to above expression, we find that slenderness ratio is not to exceed 0.62 and 1.77 for flatbars and L-profiles, respectively. For comparison, slenderness of designed frames is given in Table 2. Notice, that designed flatbars are slenderer than allowed by IACS, but consistent with the critical buckling requirement proposed recently in Ref. [11].

3.2. Load scenarios

In current design practice ice load is characterized as a uniform pressure distributed over a rectangular patch (FSICR). The nominal ice pressure p_0 is constant for all ice classes, but the applied design pressure p is varied between classes. Length of the pressure patch depends on the distance between respective structural members assuming uniform distribution of load between frames. Consequently, we use two load definitions. First, F_{total} represents the total load applied to the structure and second, F_{frame} is the load carried by a single frame and attached plating, or in other words, load per frame:

$$F_{total} = p \cdot h \cdot S_p \tag{4a}$$

$$F_{frame} = p \cdot h \cdot s \tag{4b}$$

where S_p is the total patch length and s is the frame spacing. Both definitions are used in this paper. Two patch heights, 0.35 m and 0.1 m, are considered. Former is compliant with present IA Super class design approach and latter is a simplification of a line-like contact that has been reported to develop during ice-structure interaction [13,26,27] and is currently under consideration for future FSICR rules [3], see Fig. 4.

For both load heights, different patch lengths S_p are considered as defined in Table 3. Patch length is increased from single frame spacing (1s) to fourteen frame spacings (14s) corresponding to two times the webframe spacing of 5.6 m. Furthermore, in Table 3 "isolated" refers to the case shown in Fig. 1(b), where only response of a single frame extracted from the grillage is evaluated. The ends of the frame are fixed against all DOF, while the symmetry boundary conditions are applied along the longer plate edges as shown in Fig. 1(b) to model cylindrical bending. Although these relatively simple loading scenarios do not consider all the relevant deformation pathways, they provide a necessary intermediate step prior to development of more realistic scenario for ice-structure interaction where the interaction phenomenon is taken explicitly into account.

3.3. FE modelling and simulations

All FE simulations are performed with FE software ABAQUS 6.13–3/Explicit. Modelled structures are discretized with reduced integration shell (S4R) elements with 5 integration points through thickness and stiffness based hourglass control. Analyses are performed with a 3-bay grillage model shown in Fig. 5(a). All the stiffening members are normal to the shell. The boundary conditions are defined according to ABS Guidance Notes on Ice Class [28]. Therefore, symmetry condition is applied on the left and right plane, while in top and bottom plane all degrees of freedom except rotation around x-axis are fixed, which allows rotation about the vessel's longitudinal axes. Patch load scenarios are shown in Fig. 5(b). The analysis time was set to 2 s, during which pressure linearly increased from zero to maximum applied pressure. The computational time was reduced by mass-scaling the entire model at the

Table 3
Analysis matrix.

Notation	Patch length	Patch height	
	Sp (m)	h1 (m)	h2 (m)
1s	0.4	0.35	0.1
3s	1.2	0.35	0.1
7s	2.8	0.35	0.1
14s	5.6	0.35	0.1
isolated	0.4	0.35	0.1

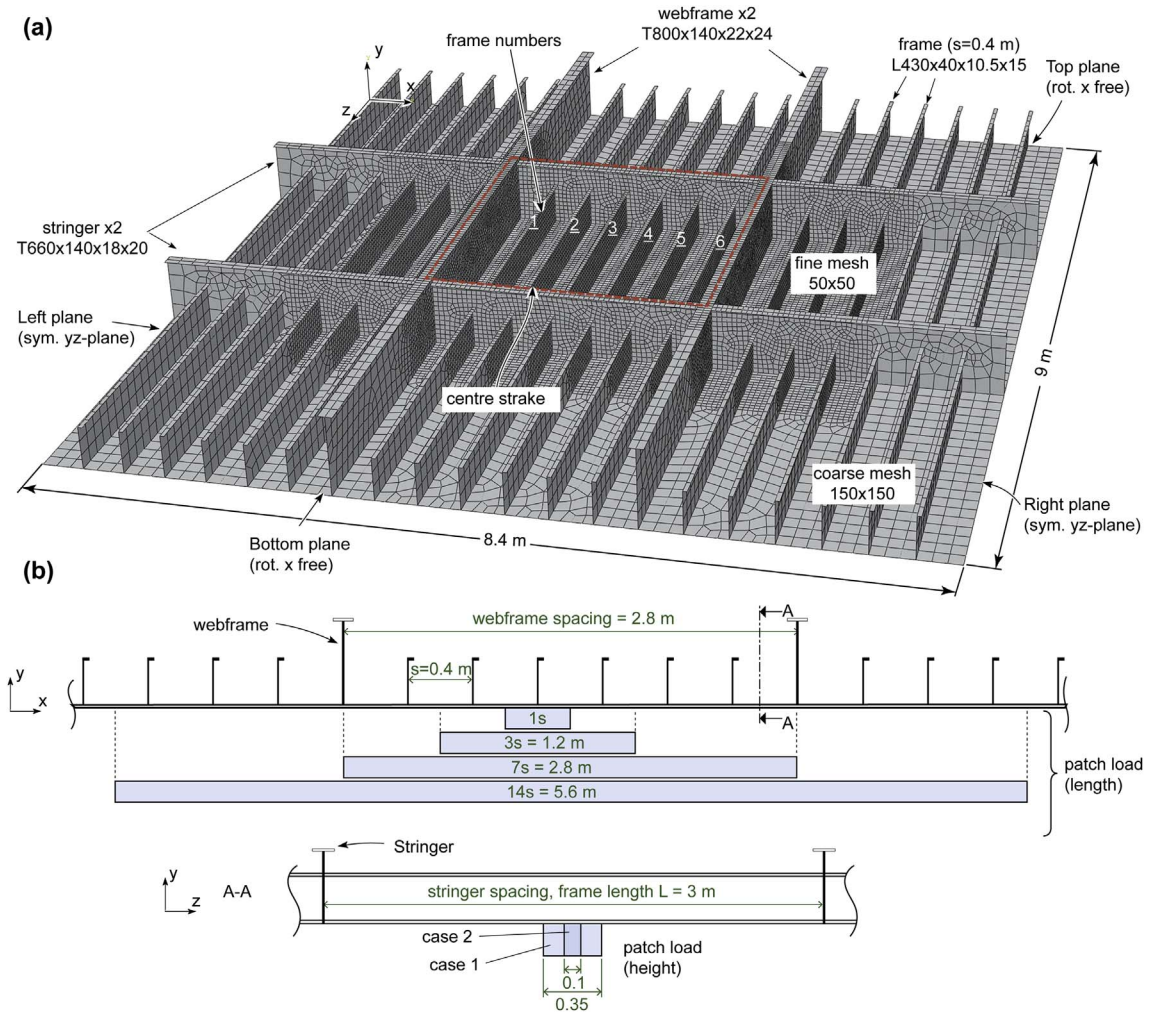

Fig. 5. (a) FE model with L-frames showing the main grillage dimensions. (b) Patch load scenarios.

beginning of the analysis by a factor of 14; the kinetic energy is below the suggested limit value of 5% of total internal energy. The pressure patches are defined on the region with refined mesh of 50 mm, whereas the rest of the model is discretized with element size of 150 mm. For clarity and consistency throughout the text, we marked the centre strake with the red boundary and numbered the frames consecutively. The equivalent stress - equivalent plastic strain ($\bar{\sigma} - \bar{\varepsilon}$) curve of the material was described with the power law

$$\bar{\sigma} = K(\bar{\varepsilon} + \varepsilon_0)^n \tag{5}$$

where $K = 680$ MPa, $n = 0.2$ and $\varepsilon_0 = 0.0127$. The elastic properties of the materials were described by a Young's modulus of $E = 206$ GPa, Poisson ratio of $\nu = 0.3$, and density of 7850 kg/m^3. Von Mises yield criterion was used in the simulations assuming associated plastic flow and isotropic hardening. No fracture criterion was used in the simulations.

4. Results and discussion

4.1. Response of grillage

The total load-deflection (F_{total}-δ) response of the whole grillage is shown in Fig. 6(a) for flatbars and in Fig. 6(b) for L-profiles. Deflection δ is measured at the mid-length of the frame ($L/2$) at the shell-frame intersection; see Fig. 2. For analyses corresponding to grillage frames (1s, 3s, 7s, 14s), this deflection is given for frame number 3; see Fig. 5(a).

It is worth noting that these figures are plotted to characterize the general response of the grillage to patch length and height variations, rather than to analyse the behaviour of individual frames. The increase in load length is accompanied by the increase in structural stiffness (slope of F_{total}-δ curve). Comparison of solid and dashed curves gives indications of load height effect, with patch height of 0.1 m leading to slightly lower capacity in all analysed cases. The curves also suggest that flatbar response is slightly more stable as the slope change is more distinctive for L-frames.

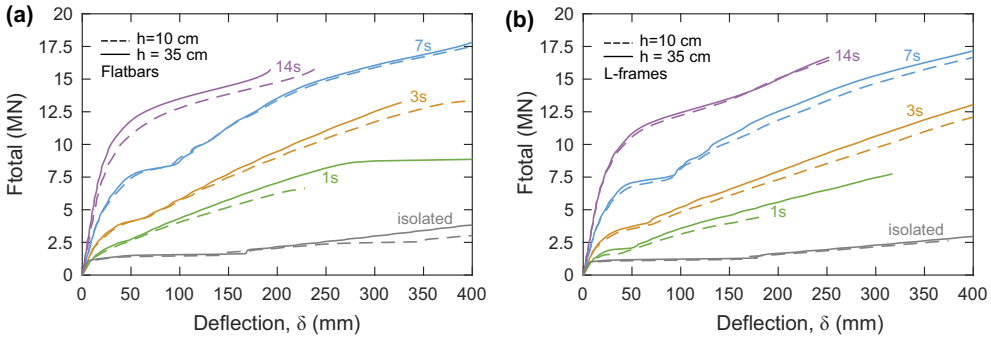

Fig. 6. F_{total}-δ curves for (a) flatbars and (b) L-frames.

4.2. Analysis of deformations

Fig. 7 shows the response of flatbar frames at deflection level of $\delta = 90$ mm and 180 mm for patch height of $h = 0.1$ m. For reason of brevity, only frames 2–4 are shown together with attached plating and stringers. The response of frames corresponding to $h = 0.35$ m is very similar, as already confirmed by Fig. 6, thus these deformations are not shown. Analogously, in Fig. 8, the corresponding pictures for L-frames are shown. Figs. 7 and 8 also include section cuts from the mid-length of the frame marked with ① that visualize deformations with respect to the initial configuration at two levels of deflection. Thereby, these section cuts convey the nature of localization due to different patches.

As already indicated by comparison in Fig. 6, flatbars in Fig. 7 exhibit a more stable bending response even at relatively high deflection level of 180 mm as opposed to L-frames in Fig. 8 that fail by combination of tripping and local web buckling. Web-end buckling on the other hand refers to the situation where web of the frame buckles in the neighbourhood of the stringer. Although web-end buckling occurs in isolated flatbar (Fig. 7(e), cross-section ②), elastic buckling of frames in grillage occurs outside of the central bay enclosed by two stringers. The buckling of frames occurs because of the compression exerted by the stringers that slightly trip (rotate) towards outer edges as a result of the applied load. Since the boundary nodes of the grillage are fixed, elastic web-end buckling occurs. Consequently, the isolated frame lacks the load sharing that is evident in grillage frame, and thus fails to mimic its behaviour.

In contrast to isolated flatbar, the isolated L-frame in Fig. 8(e) captures the local web buckling at the centre of the grillage frame with high fidelity if the patch length is relatively short (1–3 frame spacings, Fig. 8(a) and (b)). However, if the patch length increases the response becomes dominated by the web-end buckling outside the centre strake and consequent tripping of the frames. The behaviour is rationalized again with the help of boundary conditions and is similar what happens in flatbar grillage. When load is acting through a longer patch it is also more evenly distributed between frames. Each frame imparts a portion of the load to rotate the stringers similarly as in flatbar grillage. The resulting compression is sufficient to trigger elastic web-end buckling (Fig. 8(c)) prior to the local web buckling in the centre of the frame (Fig. 8(b)). Only after further increase of load web buckling occurs simultaneously in grillage frames 1–6 inside the centre strake. This contrasts with the behaviour under short patches, where only one or two frames distribute load to stringers that is insufficient to trigger web-end buckling outside the centre strake. Therefore, failure path (sequence

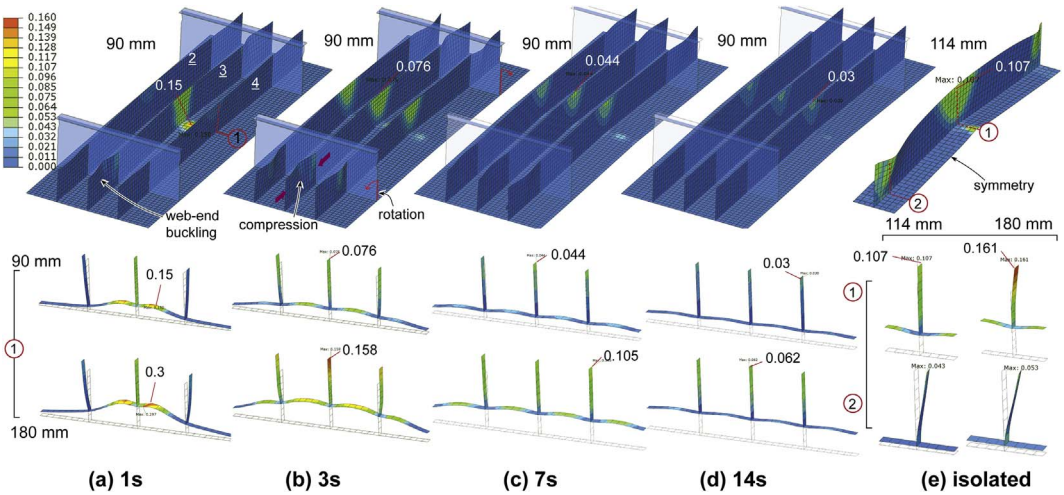

Fig. 7. Flatbar grillage response for patch height h = 0.1 m. (a) $S_p = 1$s, (b) $S_p = 3$s, (c) $S_p = 7$s, (d) $S_p = 14$s, (e) isolated frame. Colour contours show the equivalent plastic strain. (For interpretation of the references to colour in this figure legend, the reader is referred to the web version of this article.)

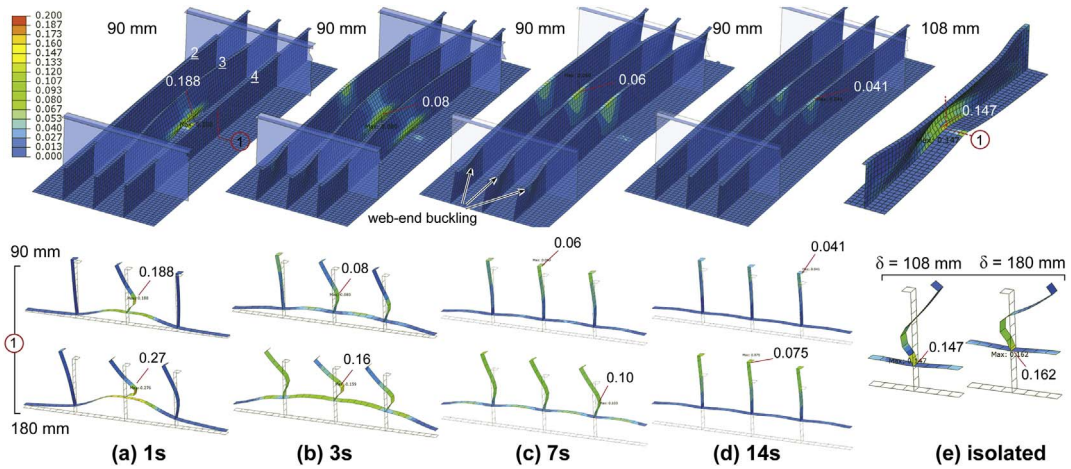

Fig. 8. L-frame grillage response for patch height h = 0.1 m. (a) S_p = 1s, (b) S_p = 3s, (c) S_p = 7s, (d) S_p = 14s, (e) isolated frame. Colour contours show the equivalent plastic strain. (For interpretation of the references to colour in this figure legend, the reader is referred to the web version of this article.)

of failure modes) in grillage is sensitive to load length, while such path-dependent failure modes cannot be obtained using isolated analysis.

We proceed by analysing under which patch lengths the grillage frame behaviour is similar to the isolated frame response under cylindrical bending and fixed boundary conditions at the frame ends. Since the shortest patch length (1s) leads to different deformation mode we separate the discussion accordingly.

(i) In case of shortest patch (1s) on flatbar grillage the cylindrical bending deformation mode is constrained by the membrane action that develops in the plate field as shown in the section cut of Fig. 7(a). Further inspection of plastic strains in Fig. 7(a) reveals that due to the membrane action, highest strains of 15% (δ = 90 mm) and 30% (δ = 180 mm), remain in the plate field. In contrast, highest strains in isolated frame (Fig. 7(e)) occur in the tip of the frame as symmetry boundary condition relaxes the constraint in the plate field that was present in grillage. Moreover, these strains in the frame tip are much smaller, 10% (δ = 114 mm) and 16% (δ = 180 mm), compared with grillage because of the early web-end buckling of the frame. In L-frame grillage (Fig. 8(a)) strains in the plate do not reach so high values because of the frame web buckling. Yet, at δ = 180 mm deflection strains in the grillage frame (Fig. 8(a)) are significantly higher than in isolated frame (Fig. 8(e)) as the biaxial stress under grillage frame leads to more localized web collapse mechanism than in isolated frame. In fact, close-up of the frames in Fig. 9 shows that the compressive stresses act along the line of developed hinge in grillage frame, while tensile stresses act in isolated frame.

(ii) The patch length increase (3s, 7s, 14s) is accompanied by the more uniform response of grillage frames as displayed by the section-cuts in Figs. 7 and 8. This uniform response across frames downgrades membrane action in the longitudinal direction (transverse to frame) to a secondary role and thus, makes the response more compliant with the cylindrical bending of isolated frames. In addition, uniform deformations invoked by longer patches are reminiscent of the "hungry horse" look wherein plate is slightly bent inwards between frames.

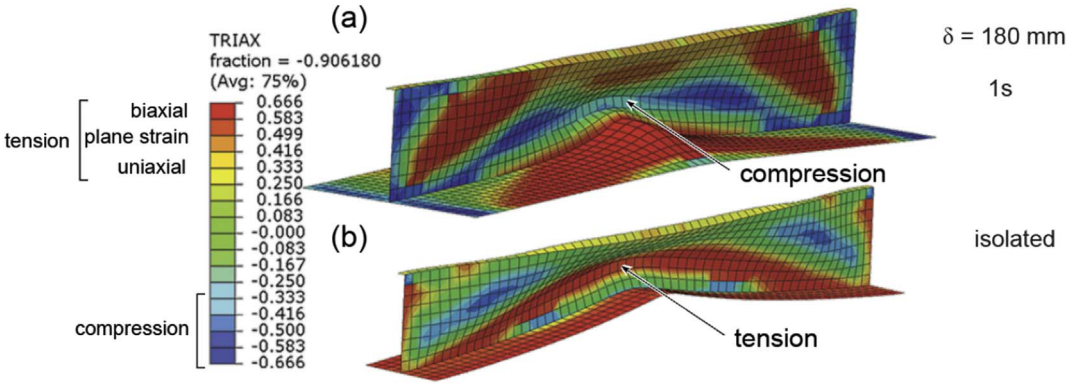

Fig. 9. Stress state comparison in L-frames at δ = 180 mm. Patch height h = 0.1 m. (a) Grillage L-frame under 1s patch. (b) Isolated L-frame.

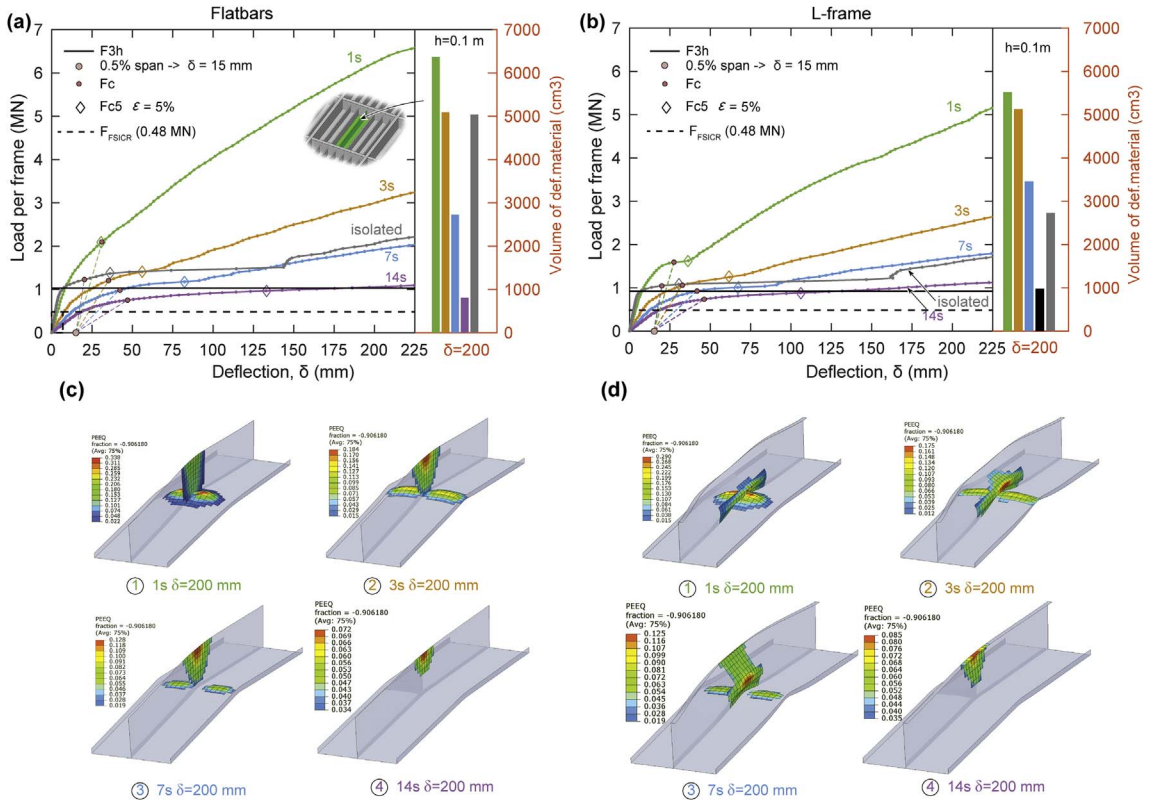

Fig. 10. F_{frame}-δ curves for (a) flatbars and for (b) L-frames when load height is $h = 0.1$ m. Second y-axis shows the volume of deformed material ($\bar{\varepsilon} > 0.05$) for a single frame shown in the inset of figure (a) at 200 mm deflection. (c–d) Grillage frames at $\delta = 200$ mm showing only the elements that are considered in the bar graphs in the top figures. Although the plate deforms plastically in all cases, plastic deformations are not revealed in case of 14s patch since plastic strains remain lower than 0.05.

4.3. Analysis of capacity against different limit states

Fig. 10(a) and (b) show the load acting on the single frame (see eq. (4b)) as a function of deflection (F_{frame}-δ) and thus, attempts to capture the behaviour of individual frames as part of the large grillage; only the results corresponding to $h = 0.1$ m are plotted as capacity was slightly lower for this more localized patch as shown in Fig. 6. Comparison with Fig. 6 further shows that the curves for 1s patch and isolated frame remain the same ($F_{total} = F_{frame}$) since the total patch length is equal with the frame spacing ($S_p = s$). The capacity of the frames is estimated using the offset method and the corresponding load F_c is denoted with the red marker and further shown in Table 4. For comparison, analytical three hinge load (F_{3h}) and design load according to FSICR (F_{FSICR}) are plotted as horizontal lines in the figure. Both are calculated with eq. (1), but load height was assumed to be $h = 0.35$ m in F_{FSICR} calculations to be consistent with rules.

Table 4 shows that maximum plastic strain varies considerably at the nominal capacity of F_c. The decrease of plastic strains with the patch length increase suggests that offset method might not recognize the actual permanent nature of deformations under longer patches where load is more distributed throughout grillage, and thus carried by elastic, rather than by plastic deformations. The volume of plastically deformed material in a single frame (frame nr 3 in grillage together with the attached plating) is displayed by the bar chart using the second y-axis in Fig. 10(a) and (b). Material is considered deformed when equivalent plastic strain is larger

Table 4
Capacity determined using two alternative methods.

Case	Flatbar, h = 0.1 m			L-frame, h = 0.1 m		
	Fc (MN)	$\bar{\varepsilon}$	*Fc5* (MN)	*Fc* (MN)	$\bar{\varepsilon}$	*Fc5* (MN)
1s	2.10	5.2%	2.1	1.57	4.5%	1.62
3s	1.20	3.4%	1.4	1.05	2.2%	1.25
7s	0.96	2.9%	1.18	0.93	2.5%	1.00
14s	0.75	1.5%	0.97	0.73	1.8%	0.88
isolated	1.22	3.7%	1.37	1.05	2.1%	1.08

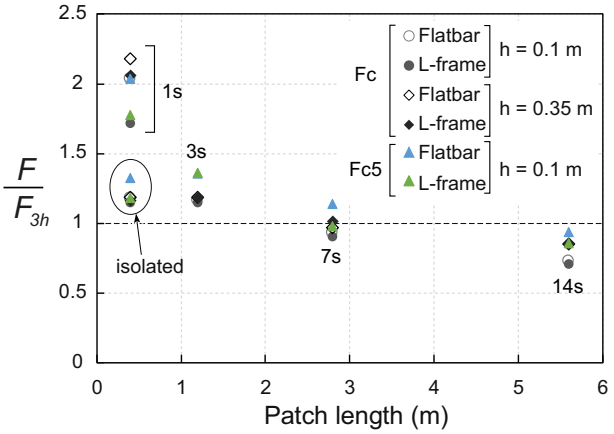

Fig. 11. Normalised capacity as a function of patch length.

than 5%. This 5% plastic strain limit was chosen based on the plastic strain at nominal capacity of 1s case, see Table 4. The placement of this deformed material in the frame is shown in Fig. 10(c) and (d). The deflection of 200 mm can be considered quite significant, but the maximum plastic strains under longest patch (14s) remain below 10%, while for the shortest 1s patch it is already in a critical range of material failure at approximately 30%.

As an alternative, more consistent measure compared to offset method, capacity is additionally ascertained at the plastic strain of $\bar{\varepsilon} = 5\%$ and denoted in Fig. 10 as F_{c5}. The values are also shown in Table 4. Both capacity levels are normalised with respect to analytical three-hinge load F_{3h} and plotted in Fig. 11. The analytical F_{3h} load provides an excellent and slightly conservative estimate for the capacity of isolated frames. This suggests that assumption made in developing the analytical expression well-characterize the actual behaviour of frames in isolation. Let us now consider grillage frames. For patch 1s, the margin of safety of grillage frame with respect to analytical value is $F/F_{3h} > 1.7$, independent of the capacity measure used. This is due to the longitudinal membrane action as discussed in the previous section. However, recall that this longitudinal membrane effect is less dominant under longer patches and thus, margin of safety should decrease if patch length increases. This is exactly what is happening in Fig. 11. For patch 3s, $F/F_{3h} = \sim 1.3$, which is the same value provided by the isolated frame analysis. When patch length is further increased (7s and 14s), the capacity reduces to levels estimated by the analytical F_{3h}, and thus analytical expression loses its conservative character. Moreover, capacity under longer patches is lower than the one given by isolated frame analysis, which is an important finding since isolated frame analysis is often considered providing a conservative estimate for the capacity.

One objective of this paper is to convey the safety margin of structures with respect to fracture. The point of fracture initiation is first analysed in terms of outer shell deflection; this relation is presented in Fig. 12. As we associated the accidental limit state (ALS) with the fracture of outer plating at the beginning of this paper, it was insightful to give deflection-strain relation separately for both, frame and plating. Therefore, after selecting the most deforming frame (frame nr. 3) and the attached plating, the maximum plastic strain at each time increment was determined for both. This implies, that the location of maximum plastic strain can change depending on the amount of deflection and thus, it explains some of the kinks observed in Fig. 12. This is more evident in L-frames where plastic strain initially developed in the flange, but after web buckling relocated to buckle that developed. For comparison, similar analysis was performed with the isolated frame. Fig. 12 shows that localization of plastic strains measured by the slope of the curves is strongest for smaller patches as already suggested by Fig. 10. To provide an insight into the safety margin against fracture, these deflection-strain relations are converted to failure maps by estimating the fracture strain ε_f using a simple fracture criterion given in DNV RP-C204 [29]:

$$\varepsilon_f = 0.02 + 0.65\frac{t_e}{L_e} \tag{6}$$

where t_e is the plate thickness and L_e the length of the plastic zone. Note that while DNV RP-C204 proposes also a critical fracture strain of 0.2 for steel S235, we used values calculated according to eq. (6). In terms of FE analyses element length provides the smallest possible length plastic strain can uniformly localize, thus L_e is equalized with the element size used in the FE simulations, i.e. 50 mm. This assumption has also been used in the literature to simulate fracture in ship collision analyses, see Ref. [30]. The corresponding fracture strain for plate and frame are plotted in Fig. 12 with horizontal lines. The key observations based on the development of plastic strain under most critical loading scenario of 1s (green curves) are:

(i) L-profiles are more critical in comparison with flatbars in terms of fracture due to their lower web thickness. Despite the web thickness effect, plastic strain also develops faster in L-frames than in flatbars. While reasons for this are not straightforward, we presume that the web buckling of L-frames impairs its ability to share load to adjacent material elements. In a sense, strains localize and get trapped in buckled folds which inhibits straining outside of these zones (local softening) as shown in Fig. 10(d) (case 1s). In contrast, during the stable bending of flatbars, a frame can gradually mobilize larger parts of itself to resist loads.
(ii) Frames are in general more critical to fracture than outer shell plating due to the same curvature at their intersection, but larger

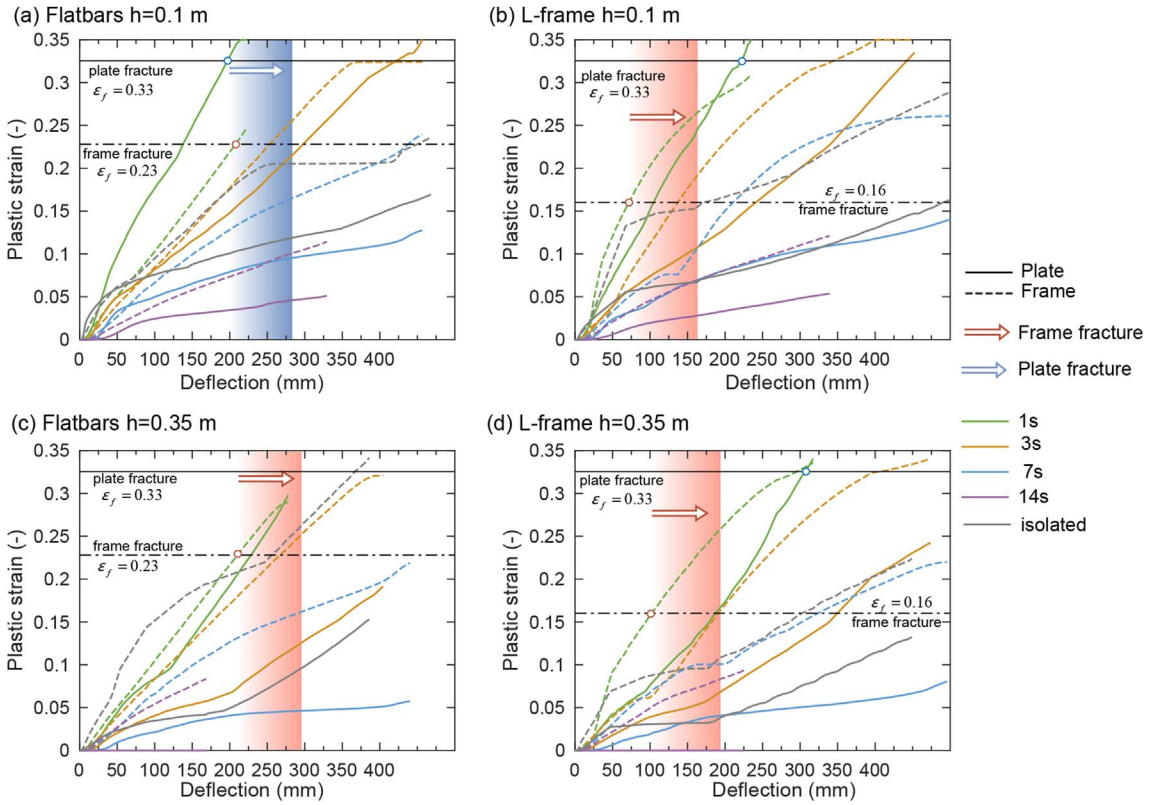

Fig. 12. Plastic strain – deflection diagrams for all analysed cases.

distance to the outer surface. However, outer shell can fracture earlier than a frame if the load height reduces (Fig. 12(a)). Moreover, the plating is more sensitive to load height variations than frames as suggested by the stronger shift of solid curves compared with dashed curves. This indicates that the stiffness and strength of plates and frames interact in very complex ways that affect the development of plastic strains.

(iii) For the combination of load scenarios, the deflection must be at least 200 mm for plate fracture to occur. This deflection is approximately the same for both L-frames and flatbars. It would be insightful to investigate how much this value is affected by the frame size.

Based on the fracture deflection limit given in Fig. 12, we can give a preliminary indication of safety margin with respect to the

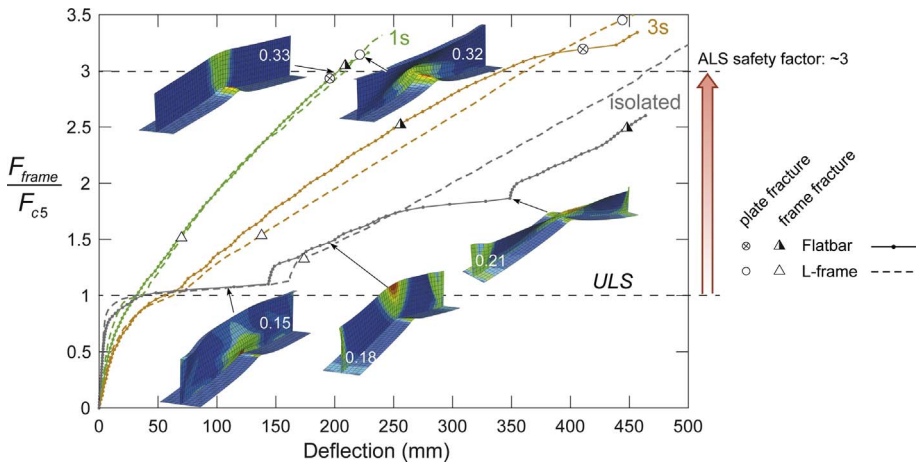

Fig. 13. Normalised frame response to show the safety margin for accidental limit state. Load height is 0.1 m. (a) Flatbars and (b) L-frames. Inset figures show the contours of plastic strains together with the maximum plastic strain in the frame.

accidental limit state of a plate fracture, which is important from general safety perspective. To this end, normalised load-deflection curves are shown in Fig. 13 for the two most critical patch scenarios (in terms of fracture) and for the isolated frame. The frame response is normalised using F_{c5} that was associated with the lower bound of the ultimate limit state (ULS) of the grillage in Fig. 2. Therefore, the safety factor with respect to design loads is expected to be higher than presented in Fig. 13. Fig. 13 shows that safety margin is in the range of ~3, but increases slightly with patch length. Moreover, another aspect that deserves attention is that L-frames provide slightly higher margin of safety than flatbars against outer shell fracture, although they exhibited lower overload capacity and limited load sharing.

5. Concluding remarks

The main contribution of this work relates to the structural overload performance of ice-strengthened ships under local ice loads as opposed to ship performance in ice. By considerations of patch length and height the most important findings and contributions relating to comparison of different modelling approaches and overload capacity until the point of failure are summarised as follows:

(i) The first finding relates to the capacity of frames under different patch length. The isolated frame analysis is often considered to yield a conservative capacity load compared with the frame that is part of the grillage [22,24]. This is true when a patch applied on the grillage frame is short (1s) as membrane effects dominate. However, longer patches suppress membrane effect and thus, capacity reduces to similar level (3s) as provided by the isolated frame analysis or even lower (7s and 14s); see Fig. 11.
(ii) According to linear elastic theory the frames carry most of the load when response remains elastic. However, at overload situations when structural behaviour becomes non-linear the load carrying mechanism changes so that increasing portion of the load is carried by the membrane stretching of the plating. Moreover, the membrane stretching (transverse to frames) of the shell plating is the key characteristic that differentiates response under short and long patches. A longer patch tends to suppress this deformation mode through more uniform, simultaneous deformation of all frames under the patch. The resulting cylindrical bending type of response is like one assumed in isolated frame analysis and in elastic theory wherein majority of the load is carried by frame bending mechanism. Hence, isolated frame behaviour is more similar to the behaviour of grillage frames under longer patches.
(iii) The local failure mechanisms of the L-frames tend to diminish the load sharing capability and so negatively affect the overload behaviour.
(iv) The offset method used to estimate capacity of frames neglects localization of deformations and thus, does not provide consistent measure for capacity under different patches. Consequently, as an alternative measure, capacity was related with equivalent plastic deformation of 5% (F_{c5}).
(v) Plastic strains – deflection diagrams show that plastic strain localizes faster in frames than in shell plating. Consequently, frames are more likely to fracture than outer shell. Shell however, is shown to be more sensitive to load height variations. Another aspect these diagrams reflect on is the complex relation between strain and deformation, which further depend on the patch size. This suggests that strain based assessment of structural limits would be difficult to implement in rule equations.
(vi) We provide failure maps where plastic strain in the structure is related to structural deformations, which upon the adoption of suitable fracture criterion, provide the estimate for the point of fracture initiation. Although fracture is not explicitly considered in simulations, the accidental limit state (ALS) event was associated with the outer shell fracture using failure maps. The safety factor against this limit state is given with respect to capacity load of F_{c5}. Although the obtained safety factors are only strictly valid for the set of assumptions and structures, the procedure presented can be applied in similar future investigations to determine safety factor against fracture. Furthermore, in future investigations safety factor could be related with easily identifiable design action such as fixed permanent deformation, rather than specific plastic strain value.

These findings are limited in several respects and thus, further research is needed concerning the following. Firstly, from the range of possible frame designs only two design alternatives are investigated following the FSICR. Consideration of different design alternatives and loading assumptions according to different rules, would provide further insight into the overload response of ice-strengthened ship structures and thus, comparative viewpoint regarding different rule assumptions. Secondly, modelled grillage structures include only the main load carrying members while excluding brackets and other reinforcements. Although important, these secondary stiffening elements would not have changed the main load carrying mechanisms between short (membrane effects) and long patches (bending dominated response). The extra stiffening on frames would certainly cause stress concentration, hinder the load spread and thus would increase the fracture susceptibility of stiffening members, as opposed to plate fracture, in these locations as exemplified in Fig. 3. The latter is consistent with our finding that frames are more fracture prone than plating, i.e. finding (v). Nevertheless, it is acknowledged that extra stiffening would have changed the load-deflection curves presented in this paper. Thirdly, the ice load is represented with a pressure distributed uniformly over a rectangular pressure patch although the actual ice-structure interaction process is considerably more complex phenomenon. While in the rules the patch size is well-defined, recent analysis by Suominen et al. [31], suggest that for the maximum load to occur on a single frame, load length must remain in the range of 1–4 frame spacings. Furthermore, this finding was based on the linear analysis and it is believed that in overload situations the shape of the patch that causes the most damage will further change. The fact that often used pressure-area relationship can shift during overload situations was also highlighted recently by Kim et al. [32]. Moreover, the pressure distribution can change considerably during ice-structure interaction similarly as ice ductility can change depending on the confinement. Consideration of these aspects is out-of-the-scope of present paper and more research is needed regarding the critical pressure distribution in overload situations.

Acknowledgments

The financial support of the Lloyd's Register Foundation, United Kingdom, is acknowledged with gratitude. The Lloyd's Register Foundation helps to protect life and property by supporting engineering-related education, public engagement and the application of research. The support from Finnish Transport Safety Agency (Trafi) is also acknowledged.

References

[1] Finnish Ministry of Transport and Communications. Communication Maritime Transport Strategy for Finland 2014–2022 2014.
[2] FSICR. Ice class regulations 2010, "Finnish-Swedish ice class rules 2010", TRAFI/31298/03.04.01.00/2010, Finnish Transport safety agency, 23.11.2010, available at www.trafi.fi.
[3] Riska K, Kämäräinen J. A review of ice loading and the evolution of the Finnish-swedish ice class rules. Proceedings of the SNAME annual meeting in Houston, Texas. November16–18, 2011.
[4] IACS. Unified requirements for polar ships: I2-structural requirements for polar class ships. International Association of Classification Societies; 2011.
[5] Kämäräinen J, Riska K. Ice class rules and international regulations. Encyclopedia of maritime and offshore engineering. John Wiley & Sons, Ltd; 2017. http://dx.doi.org/10.1002/9781118476406.
[6] Østreng W, Eger KM, Fløistad B, Jørgensen-Dahl A, Lothe L, Mejlænder-Larsen M, et al. Shipping in arctic waters. Berlin, Heidelberg: Springer Science & Business Media; 2013. http://dx.doi.org/10.1007/978-3-642-16790-4.
[7] Daley C, Kendrick A, Pavic M. New directions in ship structural regulations. 10th international symposium on practical design of ships and other floating structures (PRADS), Houston, Texas, United States of America. 2007.
[8] Wang G, Wiernicki CJ. Using nonlinear finite element method to design ship structures for ice loads. Mar Technol 2006;43:1–15.
[9] Wang G, Basu R, Chavda D, Liu S. Rationalizing the design of ice strengthened side structures. Maritime transportation and exploitation of ocean and coastal resources. Proceedings of the 11th international congress of the international maritime association of the mediterranean (IMAM 2005), Lisbon, Portugal. 26-30 September 2005. p. 549–57.
[10] Hakala MK. A nonlinear finite element analysis of an ice-strengthened ship shell structure. Comp Struct 1980;12:541–7.
[11] Daley CG, Daley KH, Dolny J, Quinton BWT. Overload response of flatbar frames to ice loads. Ships Offshore Struct 2017;12:S68–81. http://dx.doi.org/10.1080/17445302.2016.1254520.
[12] Appolonov EM, Nesterov AB, Paliy OM, Timofeev OY. A system of forming fundemental engineering solutions on assurance of ice strength and safe ship service in Russian Arctic. Proceedings of arctic shipping. 2007. St Petersburg, Russia.
[13] Izumiyama K, Takimoto T, Uto S. Length of ice load patch on a ship bow in level ice. 10th international symposium on practical design of ships and other floating structures (PRADS), Houston, Texas, United States of America. 2007.
[14] Quinton BWT, Daley CG, Gagnon RE. Realistic moving ice loads and ship structural response. Proceedings of the twenty-second international offshore and polar engineering conference rhodes, Greece, June 17–22. International Society of Offshore and Polar Engineers (ISOPE); 2012.
[15] Erceg B, Taylor R, Ehlers S. A response comparison of a stiffened panel subjected to rule-based and measured ice loads. Proceedings of the ASME 2014 33rd international conference on ocean, offshore and arctic engineering OMAE2014 June 8-13, 2014, San Francisco, California, USA. 2014.
[16] Kõrgesaar M, Kujala P. Modeling of ice loads with pressure patches in the analysis of ship structures. Arctic technology conference, october 24–26. 2016. St. John's, Newfoundland and Labrador.
[17] Daley C, Hermanski G, Pavic M. Ultimate strength of frames and grillages subject to lateral loads–an experimental study. 10th international symposium on practical design of ships and other floating structures (PRADS), Houston, Texas, United States of America. 2007.
[18] Sopper R, Daley C, Colbourne B, Bruneau S. The influence of water, snow and granular ice on ice failure processes, ice load magnitude and process pressure. 2017. p. 1–14. http://dx.doi.org/10.1016/j.coldregions.2017.04.006.
[19] ISO 19906. Petroleum and natural gas industries - Arctic offshore structures Section 7: Reliability and limit state design 2010.
[20] Smith DL. Mathematical programming methods in structural plasticity. Springer; 2014. http://dx.doi.org/10.1002/9781118476406.emoe018.
[21] Daley CG. Derivation of plastic framing requirements for polar ships. Mar Struct 2002;15:543–59.
[22] Abraham J, Daley CG. Load sharing in a grillage subject to ice loading. RINA international conference on ship and offshore technology, ice class vessels. Busan, Korea. 2009.
[23] Kujala P. Damage statistics of ice-strengthened ships in the baltic sea Winter Navigation Research Board; 1991. p. 66. Research Report No. 50, Helsinki.
[24] Lyngra NHL. Analysis of ice-induced damages to a Cargo carrier and implications wrt. Rule requirements Master Thesis Norwegian University of Science and Technology; 2014
[25] Kotisalo K, Kujala P. Ice load measurements onboard MT Uikku during the ARCDEV voyage. Proceedings of the 15th international conference on port and ocean engineering under arctic conditions. 1999. p. 974–87. august 23-27, Helsinki, Finland.
[26] Riska K, Rantala H, Joensuu A. Full scale observations of ship ice contact: results from tests series on-board IB Sampo winter 1989 Helsinki University of Technology, Laboratory of Naval Architecture and Marine Engineering; 1990.
[27] Richard M, Taylor RS. Analysis of high pressure zone attributes from tactile pressure sensor field data. ASME 2014 33rd international conference on ocean, offshore and arctic engineering ASME; 2014. http://dx.doi.org/10.1115/OMAE2014-24342. pp. V010T07A048–8.
[28] American Bureau of Shipping. ABS guidance Notes on ice class. 2014.
[29] Det Norske Veritas. DNV-RP-C204: design against accidental loads. 2010.
[30] Storheim M, Amdahl J, Martens I. On the accuracy of fracture estimation in collision analysis of ship and offshore structures. Mar Struct 2015;44:254–87. http://dx.doi.org/10.1016/j.marstruc.2015.09.006.
[31] Suominen M, Kujala P, Romanoff J, Remes H. Influence of load length on short-term ice load statistics in full-scale. Mar Struct 2017;52:153–72. http://dx.doi.org/10.1016/j.marstruc.2016.12.006.
[32] Kim E, Amdahl J, Song M. On a shifting pressure-area relationship for the accidental limit state analysis of abnormal ice actions. Progress in the Analysis and Design of Marine Structures. In: Guedes Soares C, Garbatov Y, editors. Proceedings of the 6th international conference on marine structures (marstruct 2017). 8–10 May 2017. Lisbon, Portugal.